ACS APPLIED MATERIALS & INTERFACES

Research Article

www.acsami.org

Efficient and Bright Colloidal Quantum Dot Light-Emitting Diodes via Controlling the Shell Thickness of Quantum Dots

Huaibin Shen,[†] Qinli Lin,[†] Hongzhe Wang,[†] Lei Qian,[†] Yixing Yang,[‡] Alexandre Titov,[‡] Jake Hyvonen,[‡] Ying Zheng,*[,‡] and Lin Song Li*[,†]

[†]Key Laboratory for Special Functional Materials, Henan University, Kaifeng 475004, P. R. China

[‡]NanoPhotonica Inc., 747 SW Second Avenue, Gainesville, Florida 32601, United States

Supporting Information

ABSTRACT: In this paper, we use a simple device architecture based on solution-processed ZnO nanoparticles (NPs) as the electron injection/transport layer and bilayer structure of poly(ethylenedioxythiophene):polystyrene sulfonate (PEDOT:PSS)/poly[9,9-dioctylfluorene-*co*-*N*-[4-(3-methylpropyl)]-diphenylamine] (TFB) as the hole injection/transport layer to assess the effect of shell thickness on the properties of quantum-dot-based light emitting diodes (QD-LEDs), comprising CdSe/CdS/ZnS core−shell QDs as the emitting layer. QDs with varying shell thickness were assessed to determine the best option of shell thickness, and the best improvement in device performance was observed when the shell thickness was 2.1 nm. Thereafter, different emissions of QDs, but with optimized same shell thickness (~2.1 nm), were selected as emitters to be fabricated into same structured QD-LEDs. Highly bright orange-red and green QD-LEDs with peak luminances up to ~30 000 and ~52 000 cd m^{-2}, and power efficiencies of 16 and 19.7 lm W^{-1}, respectively, were demonstrated successfully. These results may demonstrate a striking basic prototype for the commercialization of QD-based displays and solid-state lightings.

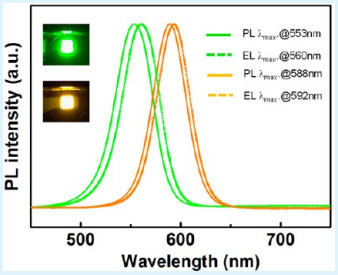

KEYWORDS: *light-emitting diodes, shell thickness, quantum dot, electroluminescence, core−shell*

1. INTRODUCTION

With the fast development of nanomaterial synthesis, especially in luminescent inorganic semiconductor quantum dots (QDs), a solid foundation which can provide high quantum efficiency (with quantum yields (QYs) > 60%), high stability, low-cost, and scalable production of QDs has been established for further research toward many important applications.[1−8] A new kind of solid state lighting device which utilizes QDs as radiant medium, usually being called quantum-dot-based light emitting diodes (QD-LEDs), has now captured many researchers' attention due to the unique characteristics such as pure color, easy emission tunability, and feasibility of solution-processability.[9−18] As recently reported by us, the red and green solution-processed (excluding electrodes) QD-LEDs with greatly improved efficiencies have been demonstrated[19] with power efficiencies of 3.8 and 8.2 lm W^{-1} for red and green devices, respectively. With inverted device structure and bias, Kwak et al.[20] demonstrated QD-LEDs with maximum luminous efficiencies of 5.7 and 19.2 cd A^{-1} for red and green devices, respectively.

It has been widely accepted that the efficiency of QD-LEDs is mainly determined by the balance between hole and electron injection rates and/or the efficient resonant energy transfer (Föster energy transfer) from transporting layers in which excitons are formed.[12,19,21−24] These two factors largely depend not only on the selection of core materials in QDs, but also on the choice of shell materials for the core−shell QD emitters and the condition of their band alignment with the charge injection layers. Generally, a core−shell structure with wide band gap shell has been used to keep stable emission from QD cores and obtain high PL QYs,[5−7] but the effect of shell thickness on the performance of QD-LEDs still remains unclear, and such effect might be very important for an in-depth understanding of the emission mechanism for QD-LEDs and thus find effective ways to improve the quality of QD-LEDs. Most recently, Pal et al.[25] reported the assessment of CdS shell on the performance of QD-LEDs comprising CdSe/CdS core−shell QDs and an improved device performance was observed as the increase of shell thickness. Therefore, the shell thickness of core−shell QD emitter and its relationships with parameters such as the EL luminance, power efficiency, external quantum efficiency (EQE), and the charge injection rates of QD-LEDs deserve intensive systematic evaluation.

Herein, we use a simple device architecture based on solution-processed ZnO nanoparticles (NPs) as the electron injection/transport layer (with the thickness of 25 nm) and bilayer structure of poly (ethylenedioxythiophene):polystyrene sulfonate (PEDOT:PSS)/poly [9,9-dioctylfluorene-*co*-*N*-[4-(3-methylpropyl)]-diphenylamine] (TFB) as the hole injection/transport layer to assess the effect of shell thickness on the properties of QD-LEDs comprising core−shell QDs as the emitting layer. QDs with varying shell thickness were assessed

Received: September 4, 2013
Accepted: November 5, 2013
Published: November 5, 2013

 © 2013 American Chemical Society

Table 1. Information for CdSe Core, Structure, Total Shell Thickness, PL Positions and QYs of Core−Shell QDs after Purification

sample	core PL peak (nm)	structure	shell thickness (nm)	PL peak (nm)	QY after synthesis (%)	QY after purification (%)
1	503	CdSe/3CdS/2.5ZnS	1.8	588	70	45
2	503	CdSe/3CdS/3.5ZnS	2.1	592	70	60
3	503	CdSe/3CdS/7.5ZnS	3.7	598	75	70
4	503	CdSe/3.5CdS/10ZnS	4.8	603	80	80

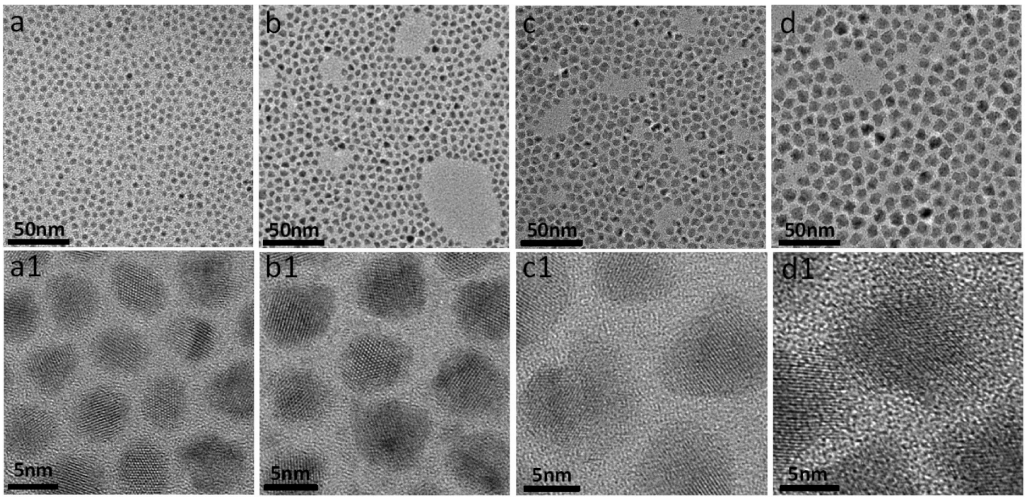

Figure 1. TEM images of CdSe/CdS/ZnS QDs corresponding with Table 1. (a) #1, 1.8 nm thickness shell (5.7 nm in diameter); (b) #2, 2.1 nm thickness shell (6.3 nm in diameter); (c) #3, 3.7 nm thickness shell (9.5 nm in diameter); (d) #4, 4.8 nm thickness shell (11.7 nm in diameter). (a1)−(d1) Corresponding HRTEM images of (a)−(d).

to determine the best option of shell thickness, and the best improvement in device performance was observed when the shell thickness was 2.1 nm. Thereafter, different emissions of QDs, but with optimized same shell thickness (~ 2.1 nm), were selected as emitters to be fabricated into same structured QD-LEDs. Highly bright orange-red and green QD-LEDs with peak luminances up to ~30 000 and ~52 000 cd m^{-2} and power efficiencies of 16 and 19.7 lm W^{-1}, respectively, were demonstrated successfully. The improvement in the balanced injection of electrons and holes into QDs contributes to the efficient exciton-involved radiative recombination within emissive QD layers, which originates from the optimization of QD shell thickness and results in high power efficiency compared with previous reports.[12,15,20,25] These results may provide helpful references for the acceleration of QD-based applications like full-color displays and solid-state lightings.

2. RESULTS AND DISCUSSION

First, we choose to evaluate device performance by using same size of CdSe cores with different thickness of shells. Presynthesized zinc blende CdSe cores with PL at 503 nm were used to grow high-quality CdSe/CdS/ZnS core−shell QDs with varying shell thickness by "green" phosphine-free method as reported in the literature.[7,26] The detailed characterization of QDs used here is described in the Experimental Section, and the results are presented in the Supporting Information. Before being used in QD-LEDs, purification of QDs was carried out. All CdSe/CdS/ZnS core−shell QDs with QY higher than 60% were obtained in solid powder form, whereas the QDs with the shell thickness of 1.8 nm were still in liquid solution due to their smaller size, with a QY of 45% after purification. The structures and optical properties of the QDs are listed in Table 1. The PL emission peaks of CdSe/CdS/ZnS core−shell QDs (in toluene) are located at 588, 592, 598, and 603 nm, respectively, with corresponding full-width at half-maxima (fwhm) ranging from 28 to 40 nm, and their corresponding transmission electron microscopy (TEM) and high resolution TEM (HRTEM) images are illustrated in Figure 1. HRTEM images of core−shell QDs indicated high crystallinity of individual QDs.

To evaluate the device properties with QDs of different shell thickness, a structure to fabricate QD-LEDs is selected and schematically shown in Figure 2a, with the devices consisting of

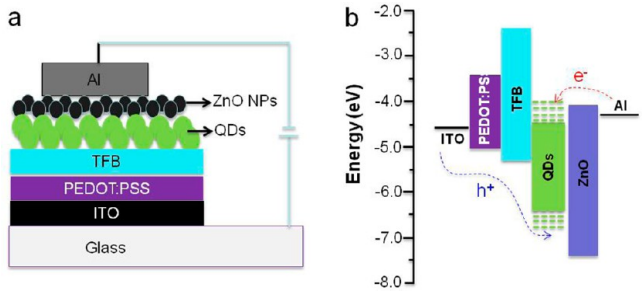

Figure 2. (a) Schematic illustration of layered QD-LEDs and (b) energy level alignment for the layers constituting QD-LEDs.

layers of indium tin oxide (ITO)/poly(ethylenedioxythiophene):polystyrene sulfonate (PEDOT:PSS) (40 nm)/poly[9,9-dioctylfluorene-*co*-*N*-[4-(3-methylpropyl)]-diphenylamine] (TFB) (30 nm)/core−shell CdSe/CdS/ZnS QDs (20 nm)/ZnO NPs (25 nm)/Al to confine the exciton formation within the QD layer. Such device structure and parameters for each layer are adopted from our previous report with a little modification of using TFB to

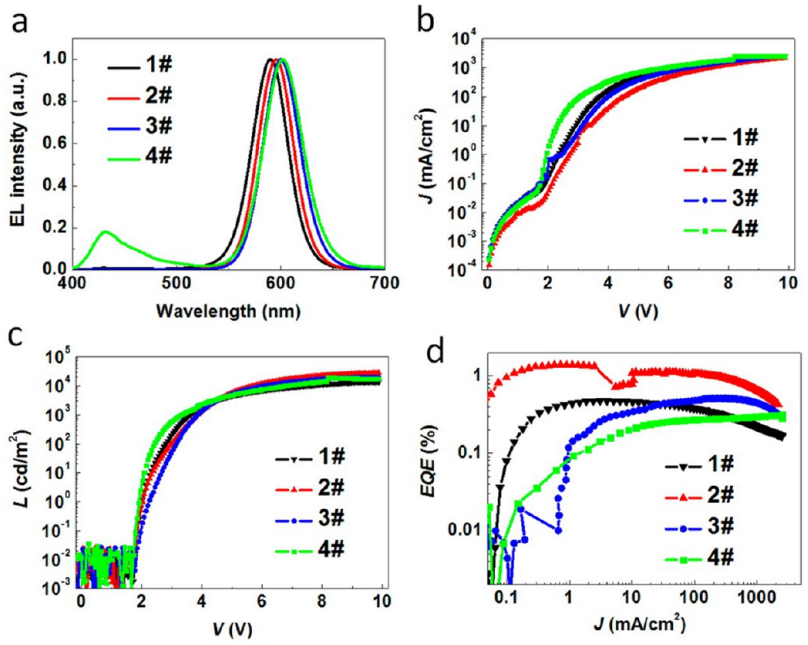

Figure 3. (a) Normalized EL spectra of QD-LEDs with different shell layers; (b) current density−voltage (J−V) plots; (c) luminance−voltage (L−V); and (d) EQE characteristics of QD-LEDs using core−shell QDs with different shell thickness as emitters.

replace Poly-TPD.[19] Since TFB possesses an even lower HOMO level than Poly-TPD, the insertion of TFB layer may doubtless reduce the barrier for the hole injection from polymers into QDs. All layers were spin-coated onto the patterned ITO substrate except for the Al cathode, which is deposited through vacuum thermal evaporation. It has been reported that the use of orthogonal solvents for adjacent layers can successfully avoid physical damage of films caused by sequential casting processes in such multilayer structures.[19]

The schematic energy level diagram of the QD-LEDs is shown in Figure 2b. The ZnO layer can provide an efficient electron injection channel as well as a hole blocking layer due to relative ideal electron affinity of ∼4.3 eV and ionization potential of ∼7.6 eV of ZnO NPs,[19] leading to an improved exciton formation and recombination within QD layer. The thickness variation of CdS/ZnS shell can influence the energy level of the core−shell QDs, and this inevitably impacts not only the emissions of core−shell QDs, but also the injection rates of holes and electrons and subsequently the luminaire efficiency of QD-LEDs.

The normalized EL spectra of QD-LEDs based on four different types of QDs listed in Table 1 are shown in Figure 3a. All the FWHMs are below 40 nm and exhibit slightly red-shifted emissions compared with corresponding PL spectra (Figure S1, Supporting Information). Major emissions originating from the CdSe/CdS/ZnS QDs were detected and no noticeable parasitic emission from adjacent TFB layer at 430 nm was observed until the shell thickness more than 4.8 nm was adopted (Figure 3a). This can be attributed to increased electron injection into TFB, which might be facilitated by the barrier formed in the path for electron injection into CdSe cores with thicker shell and the continuous shallow surface conducting path formed in the shell.

Figure 3b and c compare the current density−voltage (J−V) and luminance−voltage (L−V) characteristics of QD-LEDs with different shell thicknesses of 1.8 nm (#1), 2.1 nm (#2), 3.7 nm (#3), and 4.8 nm (#4). The J−V and L−V characterisics indicated that all four QD-LEDs showed high current density of ∼2 × 10^3 mA cm^{-2} and comparable brightness as the driving voltage approached 10 V, since such a bias was enough to eliminate the barriers formed by different shell layer thickness. However, QD-LEDs with 2.1 nm shell thickness (#2) showed the lowest current density with a driving voltage range between 2 and 8 V, whereas QD-LEDs with 1.8 nm (#1) and 3.7 nm (#3) shells showed similar current density level. This phenomenon indicates the realization of the highest exciton recombination efficiency in QD emissive layer due to balanced injections of holes and electrons. QD-LEDs with 4.8 nm (#4) shell showed the highest current density among all four devices. For instance, the current density of the #4 device reached ∼90 mA cm^{-2}, which is more than 1 order of magnitude higher than that of the #2 device, indicating the current might bypass the QD layer and cause large leakage current together with TFB emission due to less coverage of QD layer formed by large QD particles. As indicated in Figure 3c, while all four devices showed similar turn-on voltage, the #4 device showed the highest luminance in the voltage region of 2−5 V, which was supposed to be owing to the parasitic TFB emissions under low bias. The #2 device, however, displayed the highest luminance as the driving voltage went beyond 5 V, where the highest luminance of ∼28 000 cd m^{-2} was obtained at 10 V.

Since these four devices showed slightly different EL peaks, EQE would be a more objective parameter for the comparison of effects of shell thickness on device efficiency, regardless the factor of human visual perception of brightness. Figure 3d shows the EQE plots of all four QD-LEDs as a function of current density. It can be seen that as the shell thickness increased from 1.8 to 2.1 nm, improved EQE was observed across the current density range from 0.1 to 2000 mA cm^{-2}. The peak EQE reached 1.39% for the 2.1 nm shelled device versus 0.48% in the 1.8 nm shelled device. As the shell thickness exceeded 2.1 nm, the EQE decreased with increasing shell thickness, and the maximum EQE reached 0.51% and 0.30% for devices using 3.7 and 4.8 nm shelled QDs, respectively.

Therefore, it can be seen that the performance of QD-LEDs shows great dependence on the shell thickness of core−shell CdSe/CdS/ZnS QDs. Not surprisingly, core−shell QDs with 2.1 nm shells showed the highest EQE with the same core size. This trend is distinct from previous report of QD-LEDs, where different shelled CdSe/CdS QDs were used.[25] Obviously, 2.1 nm shells make the core−shell QDs reach a compromise between shell protection or exciton confinement effects and hole injection barrier induced by wide bandgap shell materials. When the thickness of shell is as thick as 4.8 nm, strong TFB emission can be observed. This implies two effects when a thicker shell over 2.1 nm is employed. On one hand, thicker shell makes the energy step between TFB and QDs a prominent blocking factor for the injection of holes into QDs. On the other hand, more continuous electron transport path is formed within thicker ZnS shell, which facilitates the electron leakage from QD to TFB. Both effects will inevitably lead to poor efficiency and bad color purity.

It is believed that the shell thickness will affect the balance in the injection of charges into the QD layer by changing electron and hole injection barrier at the charge transport layer (CTL)/QD interfaces as well as the conducting path for respective carriers. Core−shell QDs with 2.1 nm shell can provide more balanced charge injection, while too thin or too thick shells may cause imbalanced injection of electron and hole and result in reduced exciton formation and recombination efficiency. Based on the above results, the EL performance of core−shell QDs with various core emission colors but same 2.1 nm shell thickness were further investigated based on the same QD-LED structure shown in Figure 2. The composition details, PL peaks, fwhm's, and QYs of these core−shell QDs are listed in Table S1 in the Supporting Information; the corresponding TEM/HRTEM images and related powder XRD patterns are shown in Figure 4 and Supporting Information Figure S2.

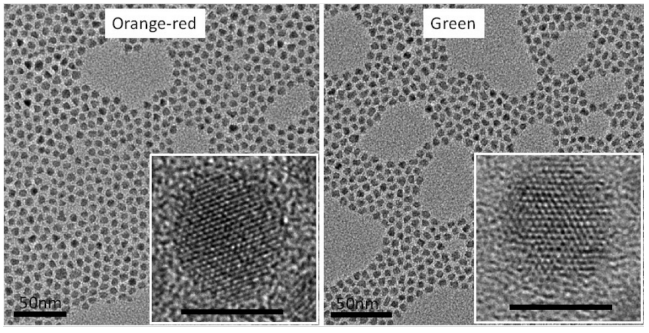

Figure 4. TEM images of QDs that correspond to Table S1 in the Supporting Information. The diameters of orange-red and green QDs are 6.3 nm. Inset: corresponding HRTEM images of core−shell QDs, indicating high crystallinity of individual QDs. Scale bars for insets are 5 nm.

The PL, EL spectra and images of the QD-LEDs are presented in Figure 5. The orange-red and green devices exhibited EL peak wavelengths at 592 and 560 nm, respectively, and no emission from TFB was observed. The emission peaks of the LEDs red-shifted by 4−7 nm in wavelength relative to their corresponding PL measured in the chloroform solution due to the Föster energy transfer in close-packed QD solids.[27] The EL fwhm's of orange-red and green QD-LEDs were measured to be 35 and 44 nm, respectively. The insets of Figure 5 show the optical photographs of orange-red and green with brightness of ~1000 cd m^{-2}.

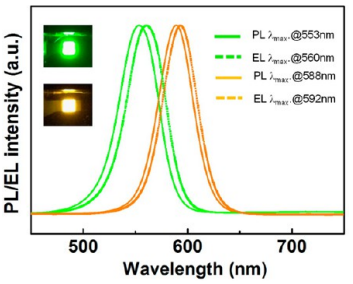

Figure 5. Normalized PL (solid lines) and EL (dashed lines) spectra of QD-LEDs. Insets: Photographs of QD-LEDs.

The current density-luminance-voltage (J−L−V) characteristics of the orange-red and green emitting QD-LEDs are shown in Figure 6. Both devices showed efficient charge injection and low turn-on voltage. The turn-on voltages (driving voltage at L = 0.1 cd m^{-2}) for orange-red and green QD-LEDs are 1.96 and 2.0 V, respectively. This is consistent with what we have observed in QD-LEDs with ZnO NPs as electron transport/injection layer.[19] The maximum luminance reaches ~30 000 and ~52 000 cd m^{-2} at driving voltages lower than 10 V for orange-red and green devices, respectively. For QD-LEDs utilizing all-solution process to fabricate transport and emission layers (i.e., except the electrodes of ITO and Al), these results can be comparable with the highest luminances for orange-red and green which have ever been reported. Due to more balanced charge injection into the QD with optimized shell thickness, improved efficiencies for both colors are achieved compared with the previous reports for QD-LEDs based on similar device architectures.[19,20] Both devices showed high power efficiencies of 16 and 19.7 lm W^{-1} for the orange-red and green, respectively (Figure 6). To the best of our knowledge, these values are the highest among the recent reports on all-solution processed QD-LEDs. The EQEs for both QD-LEDs are also shown in Figure 6. With 2.1 nm shell thickness, the maxima of EQE of 3.7% and 4.1% were achieved for orange-red and green device, respectively. Table 2 summarizes the detailed performance parameters of the two QD-LEDs in the present study. Such high luminance and efficiency of QD-LEDs is owed to the optimized matching of hole/electron injection through the appropriate choice of shell-thickness and the resulting matching of energy band alignment achieved by the existing device architecture.

3. CONCLUSION

In summary, we used a simple device architecture based on the all-solution-processable materials to assess the effects of shell thickness on the properties of QD-LEDs comprising CdSe/CdS/ZnS core−shell QDs. Significant improvements were detected in device performance when 2.1 nm of multishell was used. This improvement in the balanced injection of electrons and holes into QDs contributes to the efficient exciton-involved radiative recombination within emissive QD layers, and is supposed to originate from the choice of suitable shell material and shell thickness. Furthermore, highly bright orange-red and green QD-LEDs with fixed shell thickness of 2.1 nm have been successfully demonstrated, with maximum luminances up to ~30 000 and 52 000 cd m^{-2}, and power efficiencies of 16% and 19.7%, respectively. These results signify a remarkable progress in QD-LEDs and may offer practicable platforms for the

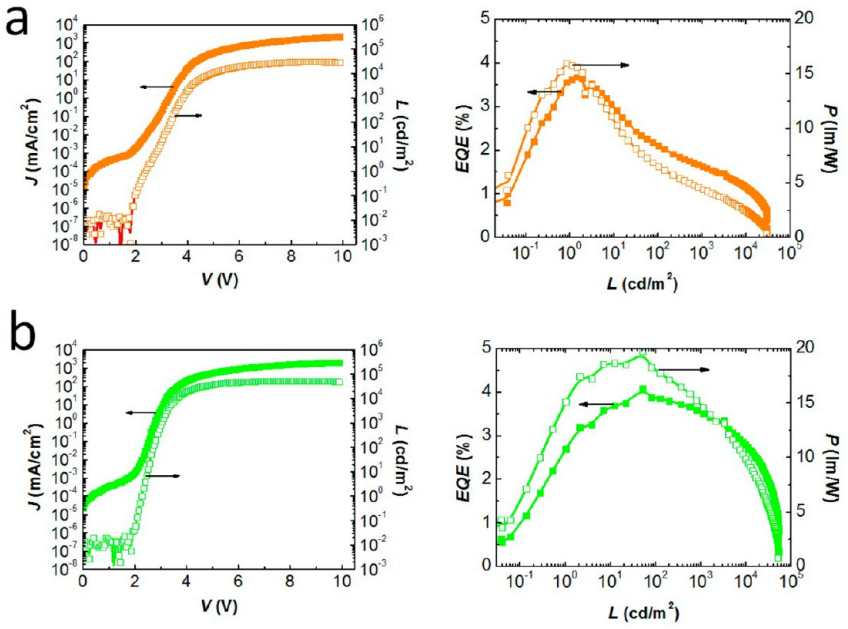

Figure 6. Plots of the measured current density–luminance–voltage (J–L–V), EQEs, and power efficiencies (P) as a function of luminance characteristics of orange-red (a) and green (b), QD-LEDs with QDs possessing an optimized shell thickness of 2.1 nm.

Table 2. Comparison of Emission Peak Wavelength (λ_{max}), fwhm (nm), Turn-on Voltage (V_T), Maximum Luminance (L_{max}), External Quantum Efficiency (η_{EQE}), Power Efficiency (η_P), and Luminous Efficiency (η_A) of QD-LEDs

color	λ_{max} (nm)	fwhm (nm)	V_T (V)	L_{max} (cd m^{-2})	η_{EQE} (%)	η_p (lm W^{-1})	η_A (cd A^{-1})
orange-red	592	35	1.96	30 000	3.7	16	12
green	560	44	2.0	52 000	4.1	19.7	16.4

realization of QD-based full-color displays and solid-state lighting.

4. EXPERIMENTAL SECTION

4.1. Synthesis of CdSe/CdS/ZnS Core–Shell QDs with Orange-Red and Green Emission. For the synthesis of CdSe core, 10 mL (1 mmol) Se precursor (see the Supporting Information) and 50 mL of paraffin oil were heated to 280 °C under nitrogen flow in a 250 mL flask. Next, 6 mL of Cd Precursor I (see the Supporting Information) was injected and temperature was lowered to 260 °C for QDs growth. The growth of shell was prepared according to the previous literature of our group.[26] A typical synthesis was performed as follows: 80 mL of ODE and 20 g of ODA were loaded into a 1000 mL reaction vessel. The CdSe QDs in hexanes (2.8×10^{-6} mol) were added, and the system was kept at 100 °C under N_2-flow for 30 min then heated up to 240 °C for the shell growth. The evolution of the absorption and PL spectra of CdSe with 13.5-layer CdSe/3.5CdS/10ZnS core–shell QDs are shown in Figure S3 (Supporting Information); corresponding TEM/HRTEM, XRD, and energy-dispersive X-ray spectroscopy (EDS) are shown in Figures S4–S6 (Supporting Information), respectively. Other emissions for CdSe/CdS/ZnS QDs were achieved by changing the thickness of ZnS shell. The evolution of the absorption and PL spectra of green emitted CdSe/1.5CdS/5ZnS core–shell QDs are shown in Figure S7 (Supporting Information).

4.2. Fabrication and Characterization of QD-LEDs. QD-LEDs were fabricated on patterned ITO coated glass substrates, and the processes were similar to those reported in our previously published reports.[21] In short, the cleaned ITO glass substrates were spin-coated with PEDOT:PSS (AI 4083) and baked at 150 °C for 15 min in air. Then, they were transferred to a N_2-filled glovebox for spin-coating of the TFB, QDs, and ZnO NP layers. ZnO NPs were obtained from NanoPhotonica, Inc. and used after being filtered with a 0.45 μm PVDF filter. TFB solution (1.5 wt %) in chlorobenzene and spin-coating process of 2000 rpm for 30 s followed by baking at 110 °C for 30 min were used for the hole-transport TFB layer. QDs (~10 mg mL^{-1}) in toluene and ZnO NPs (30 mg mL^{-1}) in ethanol were spin-coated with spin speeds of 1000 and 4000 rpm to achieve layer thicknesses of ~20 and ~25 nm, respectively. The top Al cathode (100 nm thick) was then deposited to form an active device area of 4 mm^2. Details of characterization techniques can be found in the Supporting Information.

4.3. Characterization. UV–vis absorption and PL spectra were measured with an Ocean Optics spectrophotometer (mode PC2000-ISA). PL QYs were determined by comparison of the integrated fluorescence intensity of the QD samples in solution with that of standard of known QYs (coumarin 540, QY = 78% in ethanol; rhodamine 590, QY = 95% in ethanol). TEM studies were performed using a JEOL JEM-2010 electron microscope operating at 200 kV. Phase determination of the products was carried out on an X-ray diffractometer (Philips X′ Pert Pro) using Cu Kα radiation (wavelength = 1.54 Å). EDS was performed on a Hitachi S-3400N scanning electron field emission microscope. An Agilent 4155C equipped with a calibrated Newport silicon photodetector was used to measure the current–luminance–voltage characteristics. The electroluminescence spectra were recorded using an Ocean Optics high-resolution spectrometer (HR4000).

■ ASSOCIATED CONTENT

Supporting Information

Experimental materials, preparation of precursors, detail synthesis of CdSe/CdS/ZnS core–shell QDs, TEM and HRTEM of CdSe/CdS/ZnS QDs, PL spectra of CdSe/CdS/ZnS QDs, absorption and PL spectra upon consecutive growth of CdSe/3.5CdS/10ZnS core–multishell QDs, powder XRD patterns, EDS spectra of CdSe cores, and core–shell QDs. This

material is available free of charge via the Internet at http://pubs.acs.org.

AUTHOR INFORMATION

Corresponding Authors

*E-mail: lsli@henu.edu.cn.

*E-mail: ying.zheng@nanophotonica.com.

Notes

The authors declare no competing financial interest.

ACKNOWLEDGMENTS

This work was financially supported by the research project of the National Natural Science Foundation of China (21071041 and 21201055) and Program for Changjiang Scholars and Innovative Research Team in University (No. PCS IRT1126).

REFERENCES

(1) Sanderson, K. *Nature* **2009**, *459*, 760−761.
(2) Li, L. S.; Pradhan, N.; Wang, Y.; Peng, X. *Nano Lett.* **2004**, *4*, 2261−2264.
(3) Ouyang, J.; Schuurmans, C.; Zhang, Y.; Nagelkerke, R.; Wu, X.; Kingston, D.; Wang, Z.; Wilkinson, D.; Li, Ch; Leek, D.; Tao, Y.; Yu, K. *ACS Appl. Mater. Interfaces* **2011**, *3*, 553−565.
(4) Yu, K.; Ouyang, J.; Zhang, Y.; Tung, H.; Lin, S.; Nagelkerke, R.; Kingston, D.; Wu, X.; Leek, D.; Wilkinson, D.; Li, C.; Chen, I.; Tao, Ye. *ACS Appl. Mater. Interfaces* **2011**, *3*, 1511−1520.
(5) Bae, W. K.; Char, K.; Hur, H.; Lee, S. *Chem. Mater.* **2008**, *20*, 531−539.
(6) Jun, S.; Jang, E. *Angew. Chem., Int. Ed.* **2013**, *52*, 679−682.
(7) Shen, H.; Zhou, C.; Xu, S.; Yu, C.; Wang, H.; Chen, X.; Li, L. S. *J. Mater. Chem.* **2011**, *21*, 6046−6053.
(8) Jang, H. S.; Yang, H.; Kim, S. W.; Han, J. Y.; Lee, S. G.; Jeon, D. Y. *Adv. Mater.* **2008**, *20*, 2696−2702.
(9) Colvin, V. L.; Schlamp, M. C.; Alivisatos, A. P. *Nature* **1994**, *370*, 354−357.
(10) Coe, S.; Woo, W. K.; Bawendi, M. G.; Bulović, V. *Nature* **2002**, *420*, 800−803.
(11) Leck, K.; Divayana, Y.; Zhao, D.; Yang, X.; Abiyasa, A.; Mutlugun, E.; Gao, Y.; Liu, S.; Tan, S.; Sun, X.; Demir, H. *ACS Appl. Mater. Interfaces* **2013**, *5*, 6535−6540.
(12) Sun, Q.; Wang, Y. A.; Li, L. S.; Wang, D.; Zhu, T.; Xu, J.; Yang, C.; Li, Y. *Nat. Photonics* **2007**, *1*, 717−722.
(13) Cho, K.-S.; Lee, E. K.; Joo, W.-J.; Jang, E.; Kim, T.-H.; Lee, S. J.; Kwon, S.-J.; Han, J. Y.; Kim, B.-K.; Choi, B. L.; Kim, J. M. *Nat. Photonics* **2009**, *3*, 341−345.
(14) Kim, T.-H.; Cho, K.-S.; Lee, E. K.; Lee, S. J.; Chae, J.; J. Kim, W.; Kim, D. H.; Kwon, J.-Y.; Amaratunga, G.; Lee, S. Y.; Choi, B. L.; Kuk, Y.; Kim, J. M.; Kim, K. *Nat. Photonics* **2011**, *5*, 176−182.
(15) Bae, W. K.; Kwak, J.; Park, J. W.; Char, K.; Lee, C.; Lee, S. *Adv. Mater.* **2009**, *21*, 1690−1694.
(16) Mashford, B. S.; Stevenson, M.; Popovic, Z.; Hamilton, C.; Zhou, Z.; Breen, C.; Steckel, J.; Bulović, V.; Bawendi, M. G.; Coe-Sullivan, S.; Kazlas, P. T. *Nat. Photonics* **2013**, *7*, 407−412.
(17) Wood, V.; Bulović, V. *Nano Rev.* **2010**, *1*, 5202−5208.
(18) Shirasaki, Y.; Supran, G. J.; Bawendi, M. G.; Bulović, V. *Nat. Photonics* **2013**, *7*, 13−23.
(19) Qian, L.; Zheng, Y.; Xue, J.; Holloway, P. H. *Nat. Photonics* **2011**, *5*, 543−548.
(20) Kwak, J.; Bae, W. K.; Lee, D.; Park, I.; Lim, J.; Park, M.; Cho, H.; Woo, H.; Yoon, D. Y.; Char, K.; Lee, S.; Lee, C. *Nano Lett.* **2012**, *12*, 2362−2366.
(21) Shen, H.; Wang, S.; Wang, H.; Niu, J.; Qian, L.; Yang, Y.; Titov, A.; Hyvonen, J.; Zheng, Y.; Li, L. S. *ACS Appl. Mater. Interfaces* **2013**, *5*, 4260−4265.
(22) Anikeeva, P. O.; Halpert, J. E.; Bawendi, M. G.; Bulović, V. *Nano Lett.* **2007**, *7*, 2196−2200.
(23) Coe-Sullivan, S.; Steckel, J. S.; Woo, W. K.; Bawendi, M. G.; Bulović, V. *Adv. Funct. Mater.* **2005**, *15*, 1117−1124.
(24) Anikeeva, P. O.; Madigan, C. F.; Halpert, J. E.; Bawendi, M. G.; Bulović, V. *Phys. Rev. B* **2008**, *78*, 085434−085441.
(25) Pal, B. N.; Ghosh, Y.; Brovelli, S.; Laocharoensuk, R.; Klimov, V. I.; Hollingsworth, J. A.; Htoon, H. *Nano Lett.* **2012**, *12*, 331−336.
(26) Xu, S.; Shen, H.; Zhou, C.; Yuan, H.; Liu, C.; Wang, H.; Ma, L.; Li, L. S. *J. Phys. Chem. C* **2011**, *115*, 20876−20881.
(27) Kagan, C. R.; Murray, C. B.; Bawendi, M. G. *Phys. Rev. B* **1996**, *54*, 8633−8643.